Progress In Electromagnetics Research, Vol. 143, 421–445, 2013

A WIDEBAND FREQUENCY-SHIFT KEYING MODULATION TECHNIQUE USING TRANSIENT STATE OF A SMALL ANTENNA

Mohsen Salehi[1], Majid Manteghi[1, *], Seong-Youp Suh[2], Soji Sajuyigbe[2], and Harry G. Skinner[2]

[1]Bradley Department of Electrical and Computer Engineering, Virginia Polytechnic Institute and State University, VA 24061, USA

[2]Intel Labs, Intel Corp., Hillsboro, OR 97124, USA

Abstract—The rate of wireless data transmission is limited by the antenna bandwidth. We present an efficient technique to realize a high-rate direct binary FSK modulation by using the transient properties of high-Q antennas. We show that if the natural resonance of a narrowband resonant-type antenna is switched at a high rate, the radiating signal follows the variation of resonant frequency and provides a high-rate data-transmission regardless of the narrowband characteristics of the antenna. The bit-rate in this method is dictated by the switching speed rather than the impedance bandwidth. Since the proposed technique employs the antenna in a time-varying arrangement, carrier frequencies are not required to be simultaneously within the antenna bandwidth. When demanded, the antenna is tuned to required carrier frequency according to a sequence of digital data. Moreover, if the switching frequency is properly chosen such that the stored energy in the near-zone is not dramatically disturbed, any variation in the antenna resonance will instantaneously appear in the far-field radiation due to the previously accumulated energy in the near field. Therefore, depending on the Q factor and switching speed, radiation bandwidth of the antenna can be improved independently from the impedance bandwidth. Furthermore, we show that a single RF source is sufficient to excite both carrier frequencies and the need for a VCO is obviated. Experimental results are presented to validate the feasibility of the proposed technique.

Received 22 October 2013, Accepted 18 November 2013, Scheduled 20 November 2013

* Corresponding author: Majid Manteghi (manteghi@vt.edu).

Invited paper dedicated to the memory of Robert E. Collin.

1. INTRODUCTION

Wireless communication techniques have been widely developed during the past decades due to their extensive applications. One desirable characteristic of most wireless systems is a wide bandwidth. This problem becomes significant when a high-rate data-transmission is required along with a very small-size antenna. Therefore, designing ultra-wideband (UWB) antennas which are capable of transmitting high data-rate information while occupying a small volume, is one of the challenges that has drawn a great deal of attention. For instance, biomedical implants are among the most critical devices that are required to be shrunk in the size while transmitting high data-rate information. Particularly, devices that interact with the nervous systems such as cochlear and visual prostheses need to transmit a large amount of data in order to provide high-resolution sensing for the user [1–3]. Even though a high data-rate can be achieved in broadband systems by increasing the carrier frequency, in low-frequency applications such as biomedical implantable devices, wideband data-transmission remains an open challenge. It is well-understood that in linear time-invariant (LTI) structures, antenna bandwidth is in contradiction with the size. Hence, small-size antennas suffer from narrow bandwidth [4–6]. Our team has been involved in research to break through the fundamental limits of antennas by using nonlinear time-variant techniques [7–13].

The technique proposed in this paper employs an antenna in a time-varying fashion such that the data-rate is not correlated to the traditional definition of the impedance bandwidth. We show that for a high-Q antenna, if the fundamental natural resonance is shifted over the time, the electromagnetic fields that construct the stored energy in the near-zone simultaneously shift to a new resonant frequency. Since the radiative power is tightly coupled to the stored energy of the antenna, far-field radiation responds to any abrupt variation of the antenna resonant frequency provided that the total stored energy doesn't decay dramatically. Therefore, if the resonant frequency of the antenna is switched at a high rate, a fast frequency-shift keying (FSK) modulation can be directly realized. We also show that a high-Q antenna can be used in the transient mode by imposing initial conditions on the current distribution and therefore, a single RF source is sufficient to excite both resonant frequencies when operating in the transient mode. Hence, an FSK signal can be generated and transmitted by exciting the antenna by only a single-tone source without needing to use a VCO.

To demonstrate this idea, we utilize a high-Q miniaturized antenna

loaded by switched capacitors as tuning elements. In order to provide a comprehensive analysis, we first study the transient characteristics of a high-Q switched-resonator as an equivalence of small antennas. We show that if a reactive component in a high-Q resonator which is matched and fed at frequency f_1 is switched to a different value, the frequency of the voltage waveform at the resistive load shifts to a new resonant frequency, f_2, as well. Thus, the frequency can be modulated by the switching signal which is coded by a sequence of digital data and an FSK modulation can be generated directly by the antenna. The maximum realized bit-rate is therefore a function of switching rate rather than impedance bandwidth of the antenna.

In Section 2, we present an analogy between a resonant-type antenna and its equivalent circuit model in the time domain and show that the transient characteristics of the antenna can be mimicked by the circuit model. In Section 3, the principles of switched resonators are studied. The proposed direct modulation technique is presented in Section 4. Experimental results are given in Section 5 in order to validate the simulation results. Full-wave simulations in this paper are carried out in CST Microwave Studio while Agilent ADS is used to perform the transient circuit simulations.

2. CIRCUIT MODEL FOR SMALL ANTENNAS

Modeling the antennas by lumped-element equivalent circuit has been extensively studied. Wheeler [14] introduced the concept of LC circuit equivalence in a parallel or series arrangement for TM_{01} and TE_{01} modes, respectively. Schaubert [15] applied Prony's method to Time-Domain Reflectometer (TDR) data to synthesize a rational function with real coefficients that describes the input impedance of the antenna as the summation of poles. Schelkunoff [16] introduced a general representation of impedance functions based on an arbitrary number of resonant frequencies and developed a wideband equivalent circuit. Kim and Ling [17] used a rational-function approximation in conjunction with Cauchy method [18] to find the coefficients by using the frequency-domain data. Also, the Singularity Expansion Method (SEM) [19] and Method of Moments (MoM) [20] have been used to derive equivalent circuit for antennas. Many different approaches to find broadband equivalent circuit for antennas have been proposed as well [21–26].

Nevertheless, high-Q small antennas excite only one spherical mode and the input impedance can be matched only at the fundamental resonant frequency. A self-resonant small antenna can be represented by an RLC circuit. Although an equivalent circuit is found by mimicking the input impedance of the antenna by that of an

RLC circuit, transient properties of the radiated fields such as damping factor (or time constant) are also similar to those of the circuit model. Since the radiation resistance of the antenna is lumped into a resistor, one can compare the radiated fields of an antenna excited at the nth resonant mode with the load voltage of an equivalent RLC circuit that is tuned to the resonant frequency of the antenna and resembles the antenna input impedance. Figure 1 shows an antenna that operates in a single resonant mode (nth mode) and its equivalent circuit with the same input impedance. Current distribution on the antenna surface for the tuned mode can be expressed as:

$$\mathbf{J}_n\left(\mathbf{r}', s\right) = \frac{\mathbf{J}_n\left(\mathbf{r}'\right)}{(s - s_n)(s - s_n^*)} \tag{1}$$

where s_n and s_n^* are the unloaded conjugate poles associated with the nth resonance of the antenna, and $\mathbf{J}_n(\mathbf{r}')$ is the spatial current distribution. Assuming that the current distribution is known, electric far field can be expressed as:

$$\begin{aligned}\mathbf{E}_n\left(\mathbf{r}, \mathrm{s}\right) &= \frac{\mu}{4\pi r}\int_{S'} s \cdot \mathbf{J}_n\left(\mathbf{r}', s\right) e^{-\frac{r - \hat{\mathbf{r}}\cdot\mathbf{r}'}{c}s} dS' \\ &= \frac{\mu}{4\pi r}\frac{s}{\left(s - s_n\right)\left(s - s_n^*\right)}\int_{S'} \mathbf{J}_n\left(\mathbf{r}'\right) e^{-\frac{r - \hat{\mathbf{r}}\cdot\mathbf{r}'}{c}s} dS'\end{aligned} \tag{2}$$

Equation (2) denotes that the electric field in the far-field zone has the same poles as the surface current. These poles can be found by using the equivalent RLC circuit as depicted in Figure 1(b). Input current and the input impedance of the RLC circuit can be expressed as:

$$I_{in} = \frac{V_s}{R_s + Z_{in}} \tag{3}$$

$$Z_{in} = \frac{\frac{1}{C}s}{(s - s_n)(s - s_n^*)} \tag{4}$$

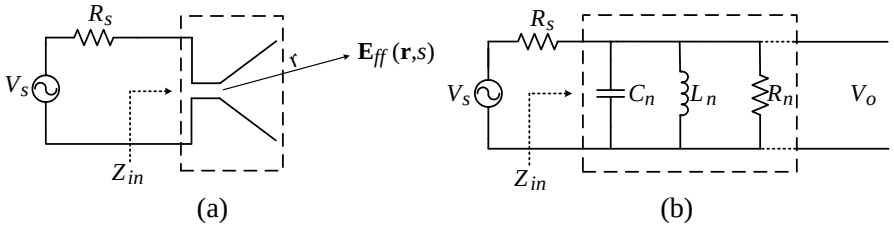

Figure 1. (a) A single-mode excited antenna and (b) equivalent circuit model.

where:

$$s_n = -\frac{\omega_{0n}}{2Q_n} + j\omega_{0n}\sqrt{1 - \frac{1}{4Q_n^2}} \tag{5}$$

ω_{0n} and Q_n are the resonant frequency and unloaded Q factor of the circuit and are defined as:

$$\omega_{0n} = \frac{1}{\sqrt{L_n C_n}}; \quad Q_n = R_n C_n \omega_{0n} \tag{6}$$

The load voltage can be now expressed as:

$$V_o = Z_{in} \cdot I_{in} = \frac{\frac{1}{R_s C} s \cdot V_s}{\left(s - s_{n_{\text{loaded}}}\right)\left(s - s^*_{n_{\text{loaded}}}\right)} \tag{7}$$

where loaded poles are:

$$s_{n_{\text{loaded}}} = -\frac{\omega_{0n}}{2Q_{n_{\text{loaded}}}} + j\omega_{0n}\sqrt{1 - \frac{1}{4Q^2_{n_{\text{loaded}}}}} \tag{8}$$

$Q_{n_{\text{loaded}}}$ is the loaded quality factor, and is equal to $Q_{n_{\text{loaded}}} = (R_n \parallel R_s)C_n\omega_{0n}$. Equation (8) gives the electric far-field poles of any arbitrary small antenna that operates in single mode at resonant frequency, ω_{0n}, with corresponding Q factor, $Q_{n_{\text{loaded}}}$. The equivalent circuit model can be constructed based on simulated or measured input impedance. Since the poles of the modal currents are preserved in the far zone, the equivalent circuit can be employed to evaluate the transient characteristics of the antenna in the far field. Even though the circuit model doesn't account for the time delay, free-space loss nor directional aspects of the radiation such as polarization and directivity, these parameters don't contribute to the radiation poles and affect only the residue of each pole, i.e., magnitude of the electric fields. Moreover, electric near-field can be also represented by the same poles. Generally, if the current distribution is expanded by the antenna's natural poles, any time-derivation or integration of Maxwell's equations will not impact the location of the poles. In other words, damping factor of the fields for each resonant mode is identical at any measurement point.

Equation (8) suggests that the damping factor for the electric fields of the nth resonance is equal to:

$$\alpha_n = \frac{\omega_{0n}}{2Q_{n_{\text{loaded}}}} \tag{9}$$

In small antennas with $Q \gg 1$, Q can be well approximated by the inverse of 3-dB impedance bandwidth as [27]:

$$Q_{n_{\text{loaded}}} = \frac{1}{\text{BW}_{3\,\text{dB}}} = \frac{f_{0n}}{\Delta f_{n_{3\,\text{dB}}}} \tag{10}$$

where $\Delta f_{n_{3\,\mathrm{dB}}} = f_{H-3\,\mathrm{dB}} - f_{L-3\,\mathrm{dB}}$. Equation (9) implies that damping factor is inversely proportional to the loaded Q of the antenna. Since at higher order resonances, electrical size of the antenna, i.e., ka, is larger, Q factor will be smaller [28]. Therefore, the lowest damping factor is associated with the fundamental mode. By combining Equations (9) and (10) one finds:

$$\alpha_n = \pi \cdot \Delta f_{n_{3\,\mathrm{dB}}} \tag{11}$$

Equation (11) shows that the damping factor of the nth resonant field can be found by knowing the absolute 3-dB bandwidth of the antenna. It should be emphasized that Equation (11) is based on the equivalent circuit model and is valid only if the antenna is narrowband such that Equation (10) holds, which is the case in a typical small-size antenna.

In order to validate Equation (11) we shall study the time-domain electric fields of two typical resonant-type antennas: dipole and Planar Inverted-F Antenna (PIFA). Figure 2 shows the antenna structures. The dipole is a half-wavelength center-fed with a diameter of 0.2 mm and the dimensions of the PIFA are $L \times W \times h = 13\,\mathrm{cm} \times 7\,\mathrm{cm} \times 5\,\mathrm{cm}$ on a $0.3\lambda \times 0.6\lambda$ ground plane. Both antennas are designed to resonate at 300 MHz. To excite the antennas, a power source matched to $50\,\Omega$ with a Gaussian pulse voltage is used in the simulations. As shown in Figure 3, the full-width at half-maximum (FWHM) of the input pulse is chosen to be $\tau_{\mathrm{FWHM}} = 1.35\,\mathrm{ns}$ to ensure that high order modes are not excited and only the fundamental resonance contributes to the radiation.

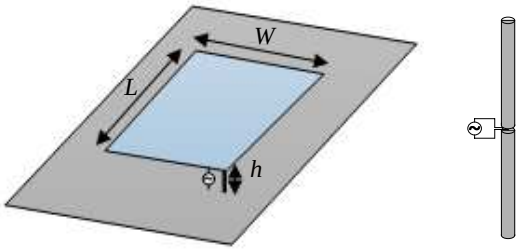

Figure 2. Simulated antenna structures: (a) PIFA and (b) half-wavelength center-fed dipole antenna

Figure 4 shows the return loss for each antenna. According to Equation (10), Q factors of the dipole and PIFA can be found about 3.9 and 22, respectively. Based on the circuit model, i.e., Equation (9) or (11), damping factor of the radiated fields for the dipole and PIFA

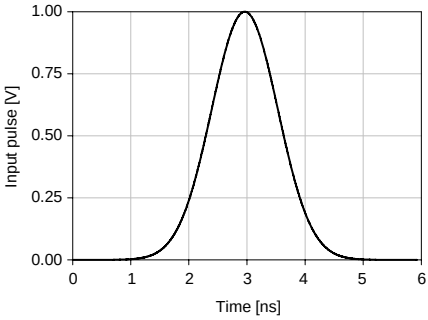

Figure 3. Input Gaussian pulse used to excite the PIFA and dipole.

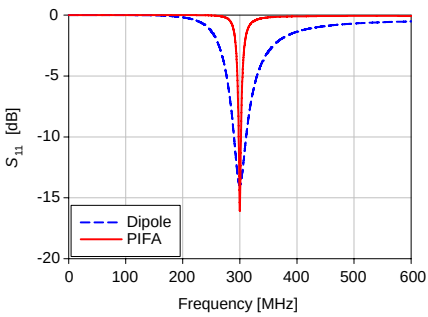

Figure 4. Simulated return loss for the PIFA and dipole.

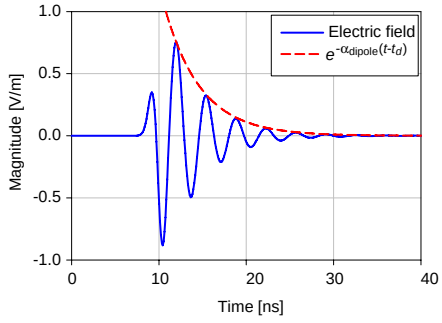

(a)

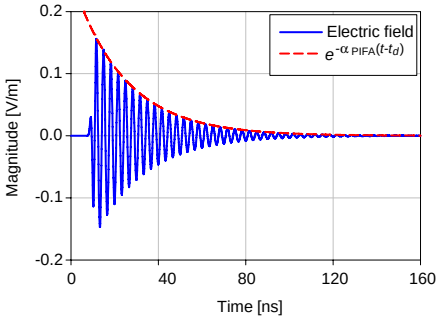

(b)

Figure 5. Time-domain z-component of the electric fields in the azimuth plane measured at 2 meters from the antennas: (a) dipole and (b) PIFA.

is $\alpha_{\text{dipole}} = 0.23/\text{ns}$ and $\alpha_{\text{PIFA}} = 0.04/\text{ns}$. Figure 5 shows the time-domain z-component of the electric fields in the azimuth plane of each antenna which is measured at a distance of 2 m from the antennas. For comparison, the decaying exponential function, $E_0 e^{-\alpha(t-t_d)}$, is shown as well. E_0 is the magnitude of the field at the first peak and t_d accounts for the travelling time delay and is set to the first peak time. As illustrated in Figure 5, damping factor of the electric fields agrees with that predicted by the circuit model. Moreover, Equation (8) indicates that the damped resonant frequency of the circuit model (transient oscillations) is approximately equal to the steady-state resonant frequency if $Q \gg 1$. Therefore, for the resonant-

type small antennas we can utilize the equivalent circuit to evaluate the transient characteristics of the antenna.

3. THE PRINCIPLES OF SWITCHED-CAPACITOR RESONATORS

Switching a reactive component in a network rearranges the location of the poles and hence, one should expect a variation in damping factor and resonant frequency after the switching instant. Since the input reactance of a switched resonator changes due to the change of a reactive component, the resonator will be tuned out with respect to the source frequency and the input impedance deviates from the matching condition. Figure 6(a) shows an RLC circuit with a switched capacitor fed by a matched source $R_L = R_S$ at frequency $f_1 = 1/2\pi\sqrt{L_1 C_1}$. At $t = t_s$, the capacitor C_2 is added to C_1 which was resonating together with the inductor L. The switched capacitor will change the steady-state resonant frequency to $f_2 = 1/2\pi\sqrt{L_1(C_1 + C_2)}$ where the new input reactance is zero and hence, the source will be mismatched with respect to the input impedance of the new circuit topology. As a result, a small fraction of the power from the source leaks into the resonator and will be dissipated in the load. If the mismatch factor is high enough, the source will be totally isolated from the resonator. However, the stored energy in the capacitor and inductor before the switching instant will be discharged to the load at a different frequency which is determined by the switched capacitor. Figures 6(b)–(c) show the equivalent topology of the circuit before and after the switching moment.

After switching, i.e., $t > t_s$, voltage at the load is composed of two frequency components. The first component is a leakage from the source at frequency f_1. Transmission coefficient from the source to the load after the switching instant can be expressed as:

$$|T| = \frac{1}{\sqrt{1 + K^2}}; \quad T = -\tan^{-1} K \tag{12}$$

where:

$$K = Q_2 \frac{f_1^2 - f_2^2}{f_1 f_2} \tag{13}$$

Q_2 is the new loaded quality factor and is equal to $\frac{R_L}{2}\sqrt{\frac{C_1+C_2}{L}}$. Equations (12) and (13) show that if either the secondary Q factor (Q_2) or the difference of the squares of f_1 and f_2 which is determined by the value of switched capacitor, C_2, is sufficiently large such that the power transmission from the source to the load is negligible, circuit

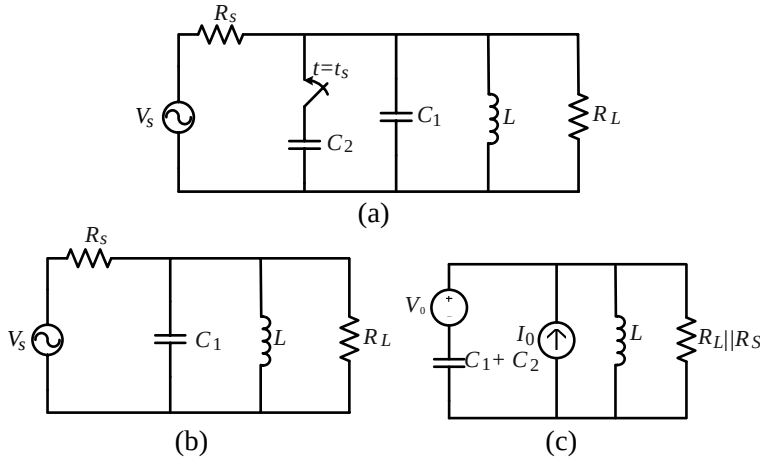

Figure 6. (a) Topology of the switched RLC circuit fed by a matched source ($R_L = R_S$) at frequency f_1 and its equivalent topologies: (b) before and (c) after the switching moment.

topology after the switching is equivalent to a source-free RLC circuit as depicted in Figure 6(c).

The second frequency component f_2 is due to a transient response produced by the initial conditions of the inductor and capacitor at the switching time. The voltage across the load according to the equivalent topology in Figure 6(c) can be expressed as:

$$v_R\left(t'\right) = e^{-\alpha t'}\left[V_1 \sin\left(\omega_d t'\right) + V_2 \cos\left(\omega_d t'\right)\right] \tag{14}$$

where $t' = t - t_s$. α and ω_d are damping factor and damped resonant frequency, respectively:

$$\alpha = \frac{\omega_2}{2Q_2}; \quad \omega_d = \omega_2\sqrt{1 - \frac{1}{4Q_2^2}} \tag{15}$$

V_1 and V_2 are determined by initial conditions and can be found as:

$$V_1 = \frac{1}{\omega_d}\left(\alpha V_0 + \frac{I_0}{C}\right); \quad V_2 = V_0 \tag{16}$$

where C is total capacitance, defined as $C_1 + C_2$, and Q_2 is the loaded quality for $t > t_s$. To find the initial conditions, one must satisfy the continuity of the electric charge and magnetic flux, i.e.,

$$q\left(t_s^+\right) = q\left(t_s^-\right); \quad \varphi\left(t_s^+\right) = \varphi\left(t_s^-\right) \tag{17}$$

From (17), V_0 and I_0 are found as:

$$V_0 = v_R\left(t_s^+\right) = \frac{C_1}{C_1 + C_2} v_R\left(t_s^-\right) \tag{18}$$

$$I_0 = i_L\left(t_s^+\right) = i_L\left(t_s^-\right) \tag{19}$$

Equation (18) indicates that in order to satisfy the charge continuity, a voltage discontinuity occurs across the capacitors to compensate the abrupt variation of the capacitance. The voltage discontinuity in turn, imposes an energy loss in the capacitors and causes the energy to be reflected back to the source. Therefore, by switching a capacitor at $t = t_s$, part of the electric stored energy in the capacitor dissipates in the source impedance. Since the inductor current is continuous according to (19), stored magnetic energy is not interrupted at the switching time and therefore, the amount of energy reduction can be expressed as the variation of stored electric energy:

$$\begin{aligned}\Delta W = \Delta W_e &= W_e|_{t=t_s^+} - W_e|_{t=t_s^-} \\ &= \frac{1}{2} C_1 \left|v_R\left(t_s^-\right)\right|^2 - \frac{1}{2}\left(C_1 + C_2\right)\left|v_R\left(t_s^+\right)\right|^2 \\ &= \frac{1}{2} C_1 \left|v_R\left(t_s^-\right)\right|^2 \left(\frac{1}{1 + C_1/C_2}\right)\end{aligned} \tag{20}$$

Equation (20) suggests that if $v_R(t_s^-) = 0$, the entire stored energy will be preserved. In fact, if the switching time is synchronous with the zero-crossing of the capacitor voltage at the switching instant, t_s, total energy is stored in the inductor in the form of magnetic energy and a capacitance discontinuity will not affect the total stored energy. Therefore, one may set the switching time such that the voltage across the capacitor is zero and the current of the inductor is maximum at the switching moment, i.e.,

$$V_0 = 0; \quad I_0 = \frac{V_s}{2L\omega_1} \tag{21}$$

Substituting these initial conditions in (16) and (14), the voltage across the load can be expressed as:

$$v_R\left(t'\right) = \frac{V_s}{2LC\omega_1\omega_d} e^{-\alpha t'} \sin\left(\omega_d t'\right) = \frac{V_s}{2} \frac{\omega_2^2}{\omega_1\omega_d} e^{-\frac{\omega_2}{2Q_2} t'} \sin\left(\omega_d t'\right) \tag{22}$$

If the resonator is high-Q ($Q \gg 1$), damped resonant frequency ω_d can be approximated by steady-state resonant frequency ω_2, according to (15) and the load voltage can be simplified as:

$$v_R\left(t'\right) = \frac{\omega_2}{\omega_1} e^{-\frac{\omega_2}{2Q_2} t'} \left[\frac{V_s}{2} \sin\left(\omega_2 t'\right)\right] \tag{23}$$

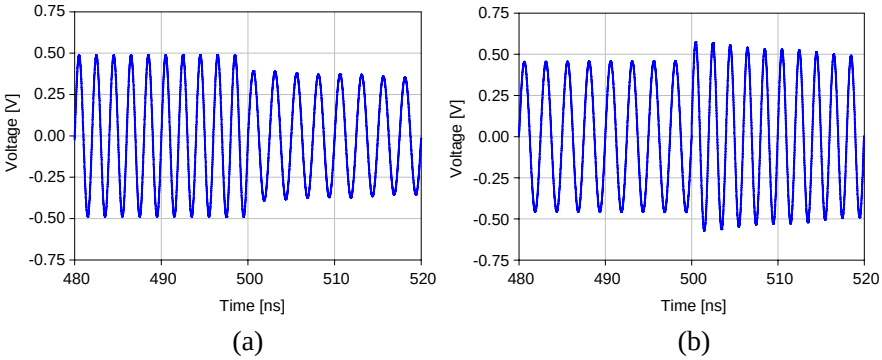

Figure 7. Voltage across the load resistor around the switching moment at $t_s = 500\,\text{ns}$, (a) the switch connects C_2 to C_1 and (b) the switch disconnects C_2 from C_1.

Figure 7 shows the voltage across the load resistor around the switching moment at $t_s = 500\,\text{ns}$ in a switched resonator with component values equal to $C_1 = 2546\,\text{pF}$, $C_2 = 1431\,\text{pF}$, $L = 39.8\,\text{pH}$ and $R_L = R_S = 50\,\Omega$. For these values, the 1st and 2nd resonant frequencies are $f_1 = 500\,\text{MHz}$ and $f_2 = 400\,\text{MHz}$ with $Q_1 = 200$ and $Q_2 = 250$.

In order to study the effect of opening and closing the switch, two cases are shown. In the first case, as shown in Figure 7(a), the source frequency is set to f_1 and at $t_s = 500\,\text{ns}$ capacitor C_2 is connected to C_1. In the second case, the source frequency is set to f_2 and at $t_s = 500\,\text{ns}$ capacitor C_2 is disconnected from C_1 and the resonant frequency shifts to f_1 as depicted in Figure 7(b). In both cases the source amplitude is 1 V.

As illustrated, right after the switching instant, resonant frequency changes according to the capacitance variations. From (23), the first peak of the transient response right after the switching occurs at $\omega t' = \frac{\pi}{2}$ and its value is equal to:

$$V_{peak} = \frac{\omega_2}{\omega_1} \cdot \frac{V_s}{2} e^{-\frac{\pi}{4Q_2}} \tag{24}$$

Since Qs are much larger than 1, V_{peak} can be approximated by $\frac{\omega_2}{\omega_1} \cdot \frac{V_s}{2}$. The amplitude of the steady-state voltage before the switching is equal to $\frac{V_s}{2}$, therefore the ratio of consequent peaks before and after the switching instant is equal to the ratio of frequencies:

$$\frac{V_{peak(>t_s)}}{V_{peak(<t_s)}} \approx \frac{f_2}{f_1} \tag{25}$$

It should be emphasized that in addition to the secondary resonant frequency after the switching moment, there is a small component in the transient response due to the imperfect mismatch between the source and the circuit topology in the transient mode. The amplitude of this component is found using (12) and (13) equal to 9 mV and 11 mV for the simulated voltage waveforms in Figures 7(a) and (b), respectively. However, since this component is much smaller than the second frequency component, one may neglect it. Damping factor of the transient response can be also calculated from (11).

It is obvious that since the absolute impedance bandwidth, $\Delta f_{n_{3\,\mathrm{dB}}}$, is inversely proportional to the Q factor at a certain resonant frequency, a high-Q resonator has a smaller damping factor. Therefore, if the resonator has a sufficiently high Q, we can switch between two frequencies according to a sequence of digital data. Due to the small decay rate in the transient mode, a frequency-shift keying (FSK) modulator can be realized by switching the capacitor ON and OFF

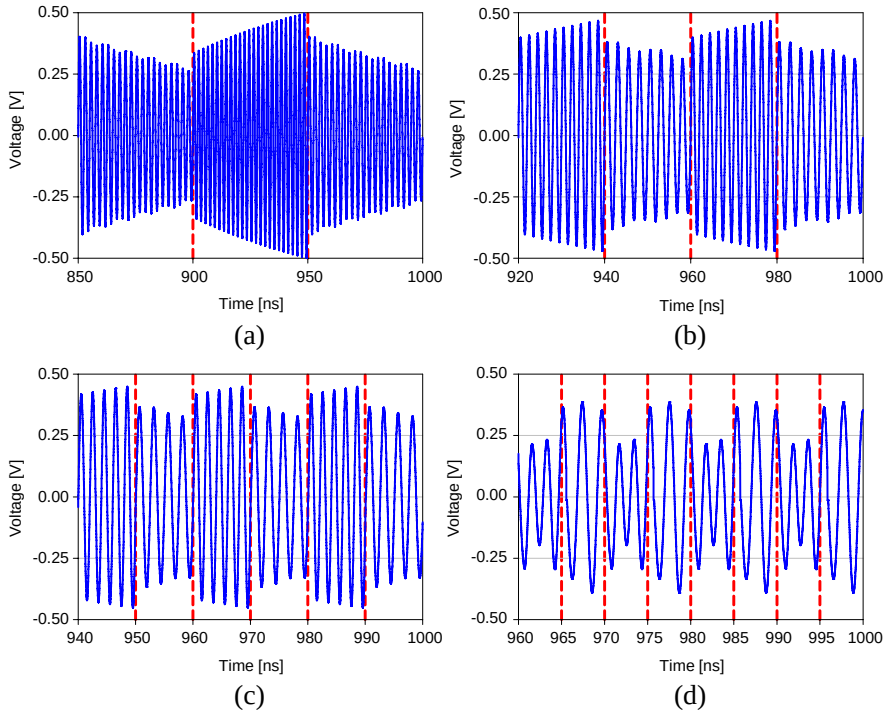

Figure 8. Load voltage for different switching frequencies: (a) 10 MHz, (b) 25 MHz, (c) 50 MHz, and (d) 100 MHz.

based on a data-coded controlling signal.

In order to preserve the stored energy, both switch-ON and switch-OFF instants should be synchronous with the zero-crossing of the capacitor voltage. In other words, the switching frequency must be a common factor of two resonant frequencies. Figure 8 shows the load voltage for different switching frequencies, 10, 25, 50 and 100 MHz. Duty cycle of the modulating pulse is 50% and each pulse represents a pair of 0 and 1 with bit duration of T_b, where $2T_b$ is the pulse period. In order to generate orthogonal FSK signals, separation between frequencies should be an integer multiplication of switching frequency $f_s = 1/T_s$ [29]. Since each switching pulse represents a pair of 0 and 1, bit-rate is twice the switching frequency. In fact, by using a fast switching mechanism, a simple narrowband RLC resonator excited by a single-tone source can be employed to generate a high data-rate FSK signal. 1st frequency is the same as the source frequency and 2nd frequency can be tuned by the switched capacitor.

4. DIRECT FSK MODULATION USING A NARROWBAND SWITCHED-ANTENNA

As discussed in Section 2, a single-mode small antenna can be modeled by an RLC resonator that mimics the antenna in both time and frequency domain. As a result, the switched-capacitor technique presented in Section 3 can be applied to a small antenna in order to realize a high bit-rate direct FSK modulation. A great benefit of employing the switched-capacitor technique to create a direct antenna modulation is that the data-rate is not limited by the antenna bandwidth. Figure 9 shows the block diagram of the direct BFSK modulation. Two capacitors, C_1 and C_2 are used to tune the antenna at f_1 and f_2, respectively. The antenna is fed at f_1 and a single pole-double throw (SPDT) switch controlled by the data sequence is used to switch between the resonant frequencies.

Starting at $t = 0$, C_1 loads the antenna and reactive energy begins to build up at frequency f_1. A portion of the energy is stored in C_1 and the rest is stored in the near-field zone of the antenna. At the moment of zero-crossing of the capacitor voltage, the switch changes its state to connect C_2 and shifts the fundamental natural resonance of the antenna to f_2. Hence, the antenna will operate in the transient mode and radiating fields shift to f_2. Since the capacitor C_1 doesn't face a voltage discontinuity, the stored electric energy is not disturbed and if the capacitor is high-Q, the entire stored energy is preserved until the next cycle of charging.

Depending on the time constant, after several cycles, stored energy

in the near-field and capacitors builds up to a maximum. During the transient operation of the antenna, the stored energy within the near-field decays slightly and provides the radiative power. The amount of energy decay depends on the Q factor of the antenna. Therefore, if the antenna has a high Q, total amount of near-field stored energy will not change dramatically and the bandwidth of the antenna will be decoupled from the stored energy, i.e., any abrupt variation in the surface current distribution will appear in the far-field momentarily, if the transmission delay is ignored.

By using a pulse train as the switch control signal where a pair of "0" and "1" can be represented by each pulse cycle, f_1 associated with C_1 represents a "1" and C_2 associated with f_2 represents a "0".

In contrast with the resonator, an antenna may excite higher order modes. Even though the higher order modes have larger damping factors, part of the input power may couple to these modes and high-order resonances appear in the radiated fields. A small antenna typically excites the fundamental mode; however, for switching application an antenna structure with only one excited natural resonance is required. Recently, an electrically-coupled loop antenna (ECLA) has been introduced as a dual for planar inverted-F antenna (PIFA) [30]. Since ECLA uses an electrically coupled feeding mechanism, further impedance matching is not required and the antenna can be highly miniaturized. As a result, the antenna can operate at a single resonance with a very high Q factor. In addition, ECLA shows excellent radiation efficiency compared to its counterpart, PIFA. These considerations make the ECLA a suitable choice for the proposed modulation technique.

Figure 10 shows the structure of ECLA. The antenna is fed via a capacitive plane (W_f) which is used to match the input impedance.

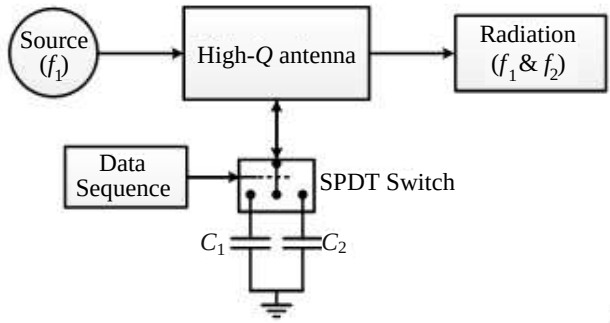

Figure 9. Block diagram of the proposed direct BFSK modulation.

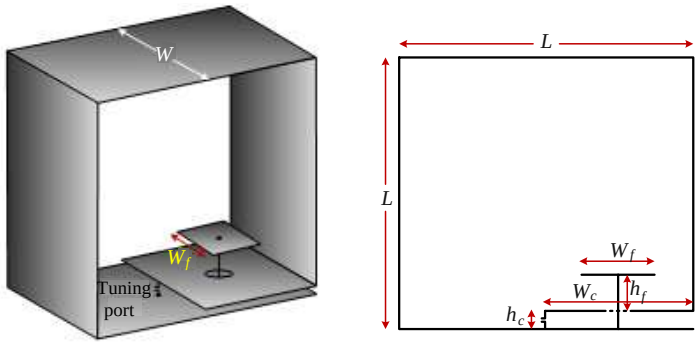

Figure 10. Structure of the electrically-coupled loop antenna (ECLA): (a) perspective view and (b) side view.

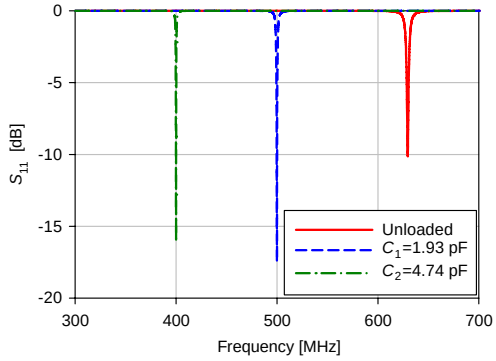

Figure 11. Return loss of a simulated ECLA with $L = 20\,\text{mm}$, $W = 15\,\text{mm}$, $w_f = 3.2\,\text{mm}$, $h_c = 0.5\,\text{mm}$, $w_c = 10\,\text{mm}$ and $h_f = 2.5\,\text{mm}$.

The loop ($L \times L \times W$) resonates along with a tunable capacitive gap (h_c) that tunes the resonant frequency and miniaturizes the antenna. In order to change the resonant frequency, the tuning port is located at the edge of the capacitive gap. Therefore, a switched capacitor can be placed in parallel with the capacitive gap and contribute to the natural resonance of the antenna. Figure 11 shows the return loss of a simulated ECLA with $L = 20\,\text{mm}$, $W = 15\,\text{mm}$, $w_f = 3.2\,\text{mm}$, $h_c = 0.5\,\text{mm}$, $w_c = 10\,\text{mm}$ and $h_f = 2.5\,\text{mm}$. The unloaded antenna resonates at $f_0 = 630\,\text{MHz}$ with 1.65 MHz 3-dB bandwidth ($Q_0 \approx 382$). The electrical dimension of the unloaded antenna is $0.04\lambda \times 0.04\lambda \times 0.03\lambda$. By loading the antenna with two capacitors

$C_1 = 1.93\,\text{pF}$ and $C_2 = 4.74\,\text{pF}$, resonant frequency can be tuned at $f_1 = 500\,\text{MHz}$ and $f_2 = 400\,\text{MHz}$ with a 3-dB bandwidth of $B_1 = 1.6\,\text{MHz}$ and $B_2 = 0.8\,\text{MHz}$ ($Q_1 = 312.5$ and $Q_2 = 500$).

Figure 12 shows the simulation set-up for the switched antenna. A small dipole is placed 1 meter away from the antenna in the E-plane to measure the electric field. The measuring dipole is aligned with the co-pol direction and terminated by a high impedance. As discussed in Section 3, in order to preserve the stored energy in the capacitors, switching moment must be synchronous with the zero-crossing of the capacitors voltage. This requires the resonant frequencies to be integer multiples of the switching frequency.

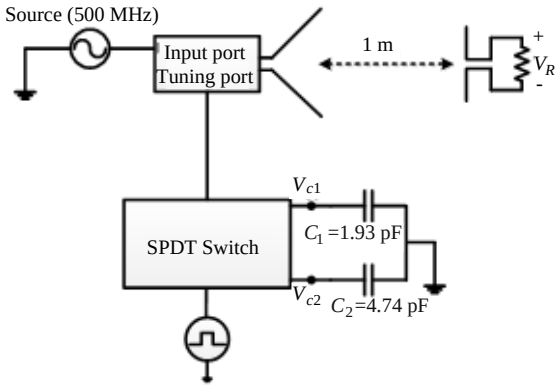

Figure 12. Simulation set-up for the switched antenna.

It is worthwhile to point out that due to the transmission-line delay, voltage zero-crossings may slightly change. This can be compensated by delaying the switch signal such that the switching moments coincide with the voltage zero-crossing of the capacitors. Figure 13 shows the voltage of the capacitors in conjunction with switching signal at 50 MHz. Since the distance between the feeding and tuning ports is small, transmission-line delay would not be significant with this configuration.

The switching signal is a two-level voltage waveform. "0" indicates the OFF state of the switch which is associated with the capacitor C_1 and frequency f_1, while "1" indicates the ON state of the switch which puts the capacitor C_2 in charge of the transient radiation at frequency f_1.

Figure 14 shows the received signal by the measuring dipole for 4 different switching frequencies: 10, 25, 50 and 100 MHz. Since each pulse represents two bits, the bit-rate is twice the switching frequency.

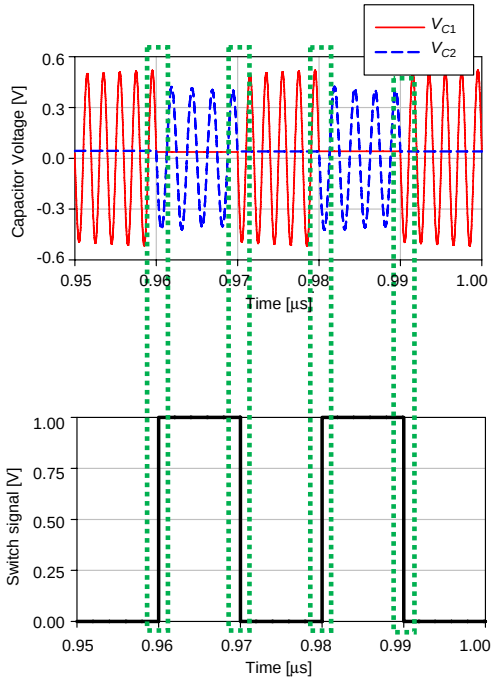

Figure 13. Voltage of the capacitors in conjunction with switching signal at 50 MHz.

It can be seen that regardless of the extremely narrow bandwidth of the antenna, bit-rate can be as high as the carrier frequency. This high bit-rate achievement is mainly due to two factors. Firstly, the time-varying property of the antenna obviates the need for covering the carrier frequency deviation, $\Delta f = f_2 - f_1$. In other words, the antenna is instantaneously tuned to f_1 and f_2 when logic "0" and "1" are to be transmitted, respectively. Secondly, since the loading capacitors change the natural resonances of the antenna, near-field reactive energy switches between different frequencies. After several switching cycles, the stored energy reaches a maximum and afterwards, the fields shift between two resonant frequencies due to variation of the antenna's fundamental resonance, resulting in radiative power shifts between the two frequencies. The nature of this frequency shifting arises from the variation of antenna poles and is not linked to the antenna input signal. Therefore, if the antenna is sufficiently high-Q and the switching moment is properly chosen such that during the transient mode the stored energy doesn't discharge dramatically and

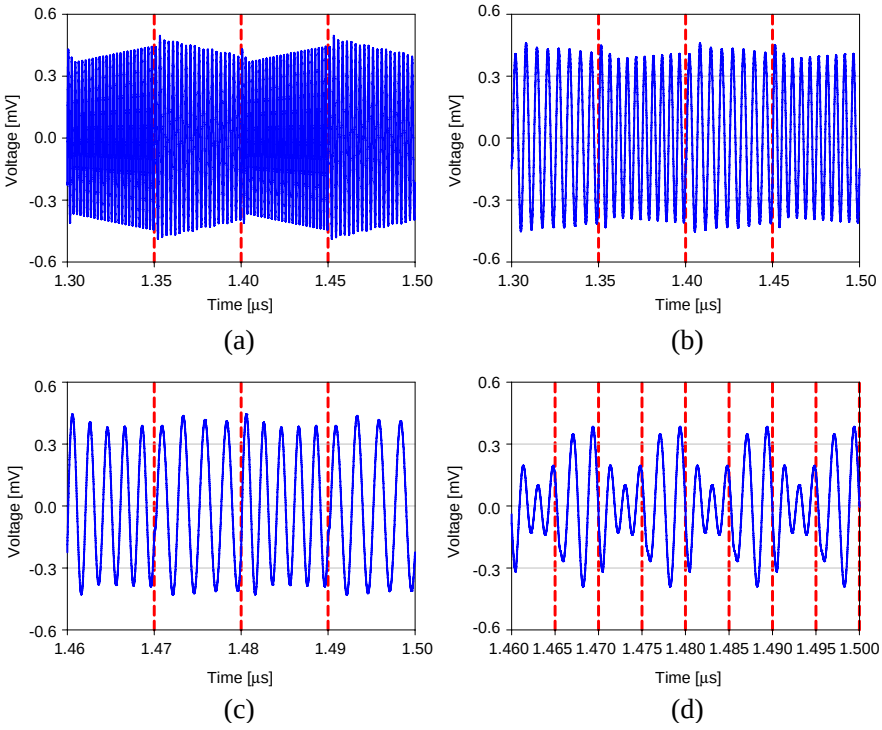

Figure 14. Simulated received signals by the measuring dipole at switching frequencies: (a) 10 MHz, (b) 25 MHz, (c) 50 MHz and (d) 100 MHz.

remains close to its maximum, the conventional impedance bandwidth will not limit the radiation bandwidth and the antenna is able to respond to any fast frequency shifting caused by switching the natural resonances.

5. EXPERIMENTAL RESULTS

To validate the proposed technique, an ECLA was prototyped and measured. The experiments are performed at a low frequency in order to implement a high-Q antenna and achieve a good isolation between the two alternating frequencies. In addition, realizing an ultra-fast and high-Q switching mechanism is a challenge as most of the commercial RF switches suffer from a relatively high insertion loss and low speed. Nevertheless, ultra-fast switching can be addressed by recently developed technologies such as SiGe transistors [31]. The

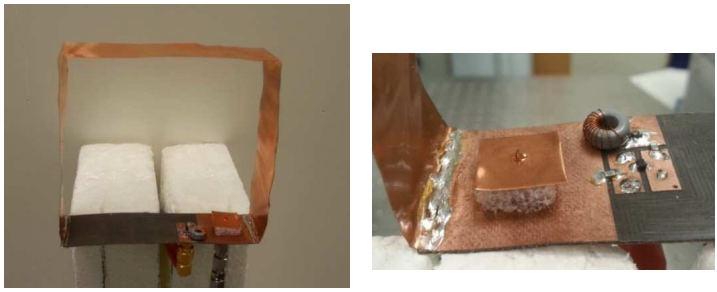

Figure 15. (a) Prototyped antenna with dimensions: $L = 100\,\text{mm}$, $W = 30\,\text{mm}$, $w_f = 25\,\text{mm}$, $h_c = 0.51\,\text{mm}$, $w_c = 30\,\text{mm}$ and $h_f = 2.5\,\text{mm}$, (b) switching circuitry attached to the antenna on a RT/Duroid 5880 with thickness 20 mil.

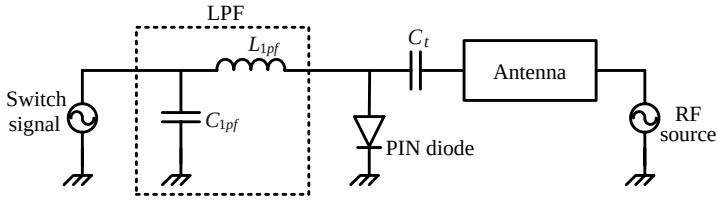

Figure 16. Switching circuitry.

prototyped antenna is shown in Figure 15 with dimensions: $L = 100\,\text{mm}$, $W = 30\,\text{mm}$, $w_f = 25\,\text{mm}$, $h_c = 0.51\,\text{mm}$, $w_c = 30\,\text{mm}$ and $h_f = 2.5\,\text{mm}$. The bottom side of the antenna that includes the switch circuitry is supported by a 20 mil Rogers RT/duroid 5880. In our experiment, we use a low-loss PIN diode (Avago HSMP-482) in a shunt arrangement as depicted in Figure 16 which shows the switching circuitry. The switching signal is separated from the antenna by a low pass filter. When the PIN diode is in reverse bias (switch-OFF), tuning port is open-circuited and the antenna is not loaded. Therefore the antenna resonates at its original resonant frequency, f_1. In the forward-bias state (switch-ON), the antenna is loaded by the capacitor C_t through a $0.6\,\Omega$ resistance of the forward-biased PIN diode and resonates at the lower frequency, f_2.

Although the capacitors and PIN diode are chip components, however due to relatively low-Q properties, particularly for the capacitors, measurement shows that the loaded Q is considerably affected. Figure 17 compares the measured return loss with the results

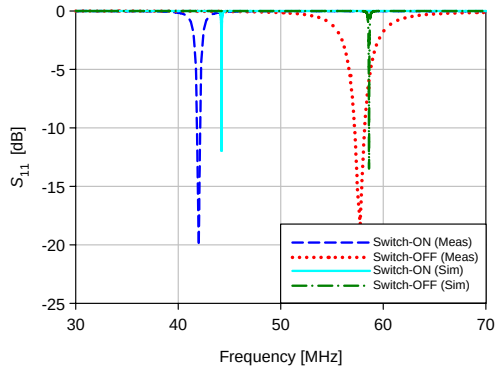

Figure 17. Measured and simulated return loss.

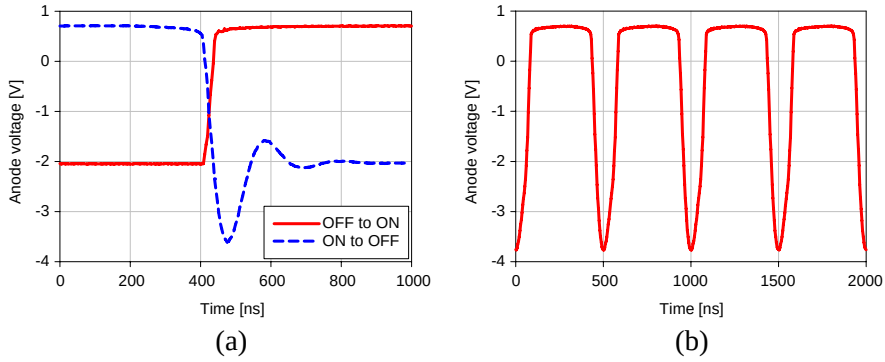

Figure 18. Measured voltage waveform across the PIN diode: (a) comparing the ON and OFF times and (b) switch signal is a 2 MHz periodic pulse varying between ±2 V with 50% duty-cycle.

of full-wave simulation that uses an ideal capacitor. The measured resonant frequencies are $f_1 = 57.75$ MHz and $f_2 = 42$ MHz where the tuning capacitor is $C_t = 47$ pF. The low pass filter with $C_{lpf} = 470$ pF and L_{lpf} =1 µH provides a suppression equal to 30 dB and 25 dB at frequencies f_1 and f_2, respectively. Measured Q factors at f_1 and f_2 are $Q_1 = 18.6$ and $Q_2 = 52.5$. The magnitude of return loss at each frequency is measured less than 0.04 dB when the antenna is tuned to the other frequency and hence the leakage is sufficiently small. Since the Q factors are still much greater than one and two resonant frequencies are well-isolated from each other, this configuration can be used to validate the proposed technique. The maximum practical

bit-rate in our experiment depends on the switching speed which is determined by the PIN diode rise and fall time. Figure 18(a) shows the measured response of the utilized PIN diode to a step-like function varying between ±2 V. The ON and OFF time based on 0 to 0.65 V and vice versa is measured about 65 ns. This limits the switching speed to about 15 MHz. Also, the PIN diode exhibits an overshoot about 1.5 times the biasing voltage at the falling edge causing the OFF time to be shortened. The switch signal measured as the anode voltage at frequency 2 MHz is shown in Figure 18(b). Even though the duty cycle of the pulse is 50%, the switch-ON duration associated with the lower frequency, f_2, is approximately twice the switch-OFF duration that represents the higher frequency, f_1.

Figure 19 shows the voltage waveform at the receiving dipole when the switched ECLA is in transmitting mode. The RF source is an R&S

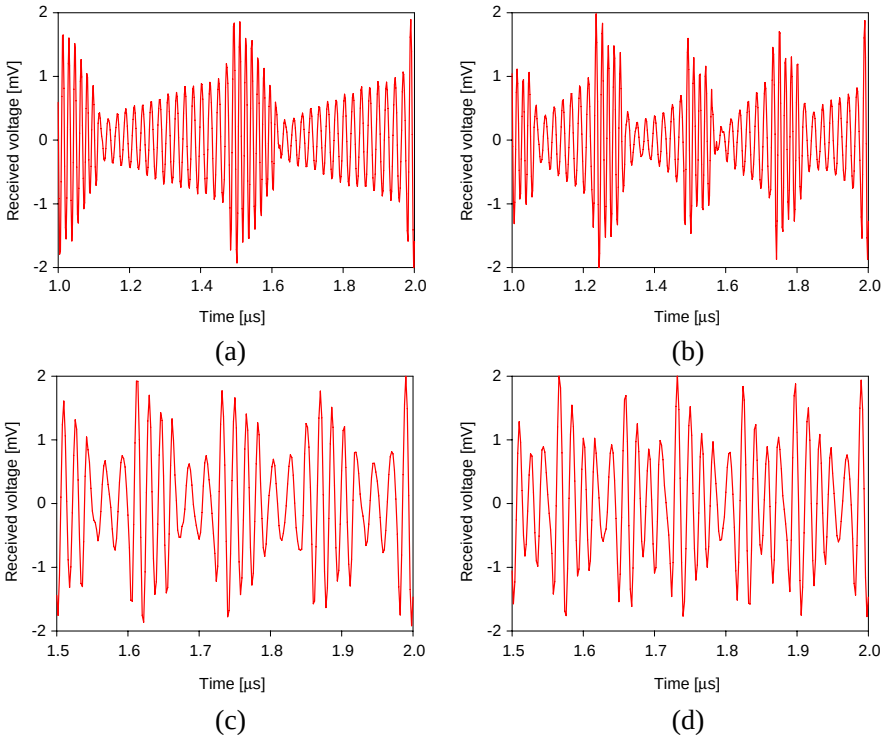

Figure 19. Measured voltage waveform received by a small dipole for different switching frequencies: (a) $f_s = 2$ MHz, (b) $f_s = 4$ MHz, (c) $f_s = 8$ MHz, and (d) $f_s = 12$ MHz.

ZVA50 vector network analyzer in the CW mode which excites the antenna at the frequency $f_2 = 42\,\text{MHz}$. A Tektronix AFG3252 signal generator is used to provide a periodic pulse as the switching signal. Time-domain electric fields are measured by a Tektronix MSO4102 oscilloscope with $1\,\text{M}\Omega$ input impedance. The electric fields shown in Figure 19 are measured at switching frequencies 2 MHz, 4 MHz, 8 MHz and 12 MHz. It can be seen that even though the antenna bandwidth is measured about 3 MHz at the upper band, an FSK modulation with a bit-rate equal to $R = 2 \times 12 = 24\,\text{Mb/s}$ is realized. The restriction on the switching frequency is due to the time constant of the low-pass filter and also the ON and OFF time of the PIN diode. Hence, the bit-rate can be further improved by using a faster switch and improving the filter performance. For demonstration purposes, the antenna has also been measured in the receiving mode. Figure 20 shows the received voltage at the input port of the ECLA when connected to a $1\,\text{M}\Omega$ oscilloscope. Both frequencies are on the air with the same power level. Similar to the transmitting mode, the switched antenna receives both frequencies according to the switching frequency.

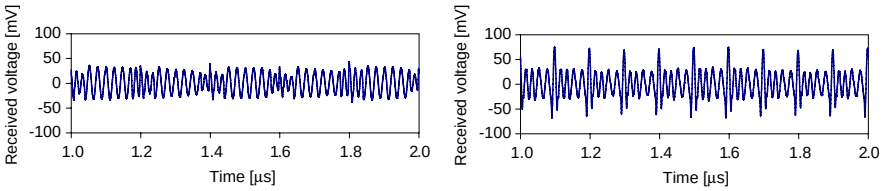

Figure 20. Measured voltage waveform received by the ECLA when operating in Rx mode at different switching frequencies: (a) $f_s = 5\,\text{MHz}$ and (b) $f_s = 10\,\text{MHz}$.

6. CONCLUSION

A new technique to realize a wideband data-transmission by using a narrowband antenna was presented. The proposed technique uses the transient property of a high-Q antenna to implement a binary FSK modulation with a high data-rate. The properties of a switched resonator was studied and it was shown that if the Q factor is sufficiently high such that the transient damping factor is small, the resonator or antenna can be switched to the transient mode and generate a binary FSK signal by using only a single source with a proper switching frequency. An electrically coupled loop antenna was prototyped and measured to validate the proposed technique.

ACKNOWLEDGMENT

This work is supported in part by Intel Corp.. The authors thank Shyam C. Nambiar for his help in preparing this manuscript.

REFERENCES

1. Ghovanloo, M. and K. Najafi, "A wideband frequency-shift keying wireless link for inductively powered biomedical implants," *IEEE Transactions on Circuits and Systems I: Regular Papers*, Vol. 51, No. 12, 2374–2383, Dec. 2004.
2. Miranda, H., V. Gilja, C. A. Chestek, K. V. Shenoy, and T. H. Meng, "HermesD: A high-rate long-range wireless transmission system for simultaneous multichannel neural recording applications," *IEEE Transactions on Biomedical Circuits and Systems*, Vol. 4, No. 3, 181–191, Jun. 2010.
3. Lee, S. B., M. Yin, J. R. Manns, and M. Ghovanloo, "A wideband dual-antenna receiver for wireless recording from animals behaving in large arenas," *IEEE Transactions on Biomedical Circuits and Systems*, Vol. 60, No. 7, 1993–2004, Jul. 2013.
4. Chu, L. J., "Physical limitations on omni-directional antennas," *Journal of Applied Physics*, Vol. 19, 1163–1175, Dec. 1948.
5. Harrington, R. F., "Effect of antenna size on gain, bandwidth, and efficiency," *Journal of Research of the National Bureau of Standards*, Vol. 64D, 1–12, Jan.–Feb. 1960.
6. McLean, J. S., "A re-examination of the fundamental limits on the radiation Q of electrically small antennas," *IEEE Transactions on Antennas and Propagation*, Vol. 44, No. 5, 672–675, May 1996.
7. Salehi, M. and M. Manteghi, "Utilizing non-linear inductors for bandwidth improvement," *URSI-USNC National Radio Science Meeting*, Boulder, CO, 2011.
8. Salehi, M. and M. Manteghi, "Bandwidth enhancement using nonlinear inductors," *2011 IEEE Antennas and Propagation Society International Symposium (APSURSI)*, 1–4, 2011.
9. Manteghi, M., "An inexpensive phased array design using impedance modulation," *URSI-USNC National Radio Science Meeting*, Boulder, CO, 2010.
10. Manteghi, M., "Non-LTI systems, a new frontier in electromagnetics theory," *2010 IEEE Antennas and Propagation Society International Symposium (APSURSI)*, 1–4, 2010.

11. Manteghi, M., "Antenna miniaturization beyond the fundamental limits," *URSI-USNC National Radio Science Meeting*, Boulder, CO, 2009.
12. Manteghi, M., "A switch-band antenna for software-defined radio applications," *IEEE Antennas and Wireless Propagation Letters*, Vol. 8, 3–5, 2009.
13. Manteghi, M., "Antenna miniaturization beyond the fundamental limits using impedance modulation," *2009 IEEE Antennas and Propagation Society International Symposium, (APSURSI)*, 1–4, 2009.
14. Wheeler, H. A., "Fundamental limitations of small antennas," *Proceedings of the IRE*, Vol. 35, No. 12, 1479–1484, Dec. 1947.
15. Schaubert, D. H., "Application of Prony's method to time-domain reflecto-meter data and equivalent circuit synthesis," *IEEE Transactions on Antennas and Propagation*, Vol. 27, No. 2, 180–184, Mar. 1979.
16. Schelkunoff, S. A., "Representation of impedance functions in terms of resonant frequencies," *Proceedings of the IRE*, Vol. 32, No. 2, 83–90, Feb. 1944.
17. Kim, Y. and H. Ling, "Equivalent circuit modeling of broadband antennas using a rational function approximation," *Microwave and Optical Technology Letter*, Vol. 48, No. 5, 950–953, May 2006.
18. Adve, R. S., T. K. Sarkar, S. M. Rao, E. K. Miller, and D. R. Pflug, "Application of the cauchy method for extrapolating/interpolating narrow-band system responses," *IEEE Transactions on Microwave Theory and Techniques*, Vol. 45, No. 5, 837–845, May 1997.
19. Michalski, K. A. and L. W. Pearson, "Equivalent circuit synthesis for a loop antenna based on the singularity expansion method," *IEEE Transactions on Antennas and Propagation*, Vol. 32, No. 5, 433–441, May 1984.
20. Simpson, T. L., J. C. Logan, and J. W. Rockway, "Equivalent circuits for electrically small antennas using LS-decomposition with the method of moments," *IEEE Transactions on Antennas and Propagation*, Vol. 37, No. 12, 1632–1635, Dec. 1989.
21. Hamid, M. and R. Hamid, "Equivalent circuit of dipole antenna of arbitrary length," *IEEE Transactions on Antennas and Propagation*, Vol. 45, No. 11, 1695–1696, Nov. 1997.
22. Love, A. W., "Equivalent circuit for aperture antennas," *Electronics Letters*, Vol. 23, No. 13, 708–710, 1987.

23. Vainikainen, P., J. Ollikainen, O. Kivekäs, and I. Kelander, "Resonator-based analysis of the combination of mobile handset antenna and chassis," *IEEE Transactions on Antennas and Propagation*, Vol. 50, No. 10, 1433–1444, Oct. 2002.
24. Tang, T. G., Q. M. Tieng, and M. W. Gunn, "Equivalent circuit of a dipole antenna using frequency-independent lumped elements," *IEEE Transactions on Antennas and Propagation*, Vol. 41, No. 1, 100–103, Jan. 1993.
25. Streable, G. W. and L. W. Pearson, "A numerical study on realizable broad-band and equivalent admittances for dipole and loop antennas," *IEEE Transactions on Antennas and Propagation*, Vol. 29, No. 5, 707–717, Sep. 1981.
26. Liu, G. K. H. and R. D. Murch, "Compact dual-frequency PIFA design using LC resonators," *IEEE Transactions on Antennas and Propagation*, Vol. 49, No. 7, 1016–1019, Oct. 2001.
27. Chu, L. J., "Physical limitations of omni-directional antennas," *Journal of Applied Physics*, Vol. 19, 1163–1175, Dec. 1948.
28. Davis, W. A., T. Yang, E. D. Caswell, and W. L. Stutzman, "Fundamental limits on antenna size: A new limit," *IET Microwaves, Antennas & Propagation*, Vol. 5, No. 11, 1297–1302, 2011.
29. Proakis, J. G. and M. Salehi, *Digital Communications*, 5th Edition, McGraw Hill, NY, 2008.
30. Manteghi, M., "Electrically coupled loop antenna as a dual for the planar inverted-F antenna," *Microwave and Optical Technology Letters*, Vol. 55, No. 6, 1409–1412, Jun. 2013.
31. Hancock, T. M. and G. M. Rebeiz, "Design and analysis of a 70-ps SiGe differential RF switch," *IEEE Transactions on Microwave Theory and Techniques*, Vol. 53, No. 7, 2403–2410, Jul. 2005.